Design and Characterization of High Efficiency Nanoantenna Couplers With Plasmonic Integrated Circuit

Qian Gao, Spencer Liverman, and Alan X. Wang

***Abstract*—Four types of nanoantennas have been designed and characterized at 1.55 μm wavelength: Dipole antenna, Yagi-Uda antenna, dipole antenna array and bowtie antenna. The spectra, coupling efficiency, and far field radiation patterns are also investigated. We also quantitatively characterized the relationship between the couple-in efficiency and the spot size of the incident light. For the three dipole-type antennas, the couple-in and couple-out efficiencies have been measured experimentally. A plasmonic integrated circuit has also been designed and fabricated with these four types of nanoantennas. Direct and efficient optical coupling from an optical fiber into the plasmonic integrated circuit is demonstrated as well, and the couple-out efficiencies for these four nanoantennas are.**

***Index Terms*—Optical couplers, optical nanoantennas, plasmonic waveguides.**

I. Introduction

FOR high-speed communication, it requires size scaling of electronic transistors and interconnect circuits to improve the operating frequencies and reduce the delay [1]. The bottlenecks of these two factors limit the maximal bandwidth. In lieu of electronic circuits, a photonic roadmap leading to ultra-compact photonic integrated circuits (PICs) shows potential for the development of next generation computation and communication systems [2]. However, it also requires photonic components to have comparable size and speed with their electronic counterparts to create, guide, and modulate optical signals. Such requirements push the scaling of photonic devices beyond the diffraction limit. One potential solution is to use surface plasmons (SPs) [3], which are electromagnetic waves that travel along the metal-dielectric interfaces. The interaction of metal with light has led to a new area of photonics called plasmonics. It has been proven that plasmonic integrated circuits are capable of guiding light beyond the diffraction limit [4]. And the exceptional ability of plasmonic devices to confine light into subwavelength scales [5] has been demonstrated in many nanophotonics technologies. In recent years, quantum emitters, such as nano light-emitting diodes (LEDs) [6] and nanolasers [7]–[10], have been developed as efficient on-chip light sources with size much smaller than the optical wavelength. Moreover, several achievements have been made in active plasmonic devices such as solar cells [11], [12], sensing and imaging [13]–[15], optical switches [16]–[18], and optical modulators [19]–[22]. Merging the aforementioned quantum emitters, active plasmonic devices and plasmonic integrated circuits may achieve unprecedented bandwidth density and ultimate functionalities. Such circuits can be applied in various fields, such as nanoscale biosensing elements [23], on-chip optical communication [24], and quantum plasmonics [25]. However, the performance of such circuits is limited by the poor energy conversion efficiency within subwavelength plasmonic waveguides. Such a challenge needs to be addressed when designing plasmonic integrated circuits.

Plasmonic slot waveguides are capable of guiding electromagnetic waves with a mode at subwavelength scale, which can potentially overcome the fundamental diffraction limit of traditional waveguides. In order to focus and convert free space light into subwavelength plasmonic waveguide, a few types of nanocouplers have been reported, such as plasmonic grating couplers [26]–[28], Luneburg lenses [29], nanoparticle couplers [30], and optical nanoantennas [31]–[32]. For instance, optical coupling with plasmonic gratings and tapered waveguides has been designed to produce surface plasmon polaritons (SPPs) and focus them into plasmonic waveguide down to 90 nm scale. The efficiency of transmission is $20 \pm 7\%$ at wavelength of 1.55 μm. Among all of those reported nanocouplers, the most compact design is the nanoantenna. It can operate as a light concentrator and a high-efficiency mode converter at the same time [33], [34]. It has been shown that the coupling efficiency can achieve 26% [35] at maximum for the dipole antennas with reflectors on the side and bottom. A Yagi-Uda nanoantenna with radiation efficiency of 60% has been implemented [36]. In addition, two bowtie antennas in series showed 10% coupling efficiency [37]. The bowtie antenna has larger size and therefore higher absorption compared with Yagi-Uda nanoantenna [38]. However, to the best of the authors' knowledge, experimental comparison of different nanoantennas and the integration on a single PIC has not been demonstrated yet. In this paper, we first present the design of four types of nanoantennas and simulation results, including far field radiation patterns, couple-in and couple-out efficiencies, and near field profiles. Then for

Manuscript received August 24, 2016; revised October 28, 2016; accepted November 15, 2016. Date of publication November 20, 2016; date of current version June 24, 2017. This work was supported in part by the National Science Foundation under Grants 1342318 and 1449383 and in part by the AFOSR MURI project under the guidance of Dr. G. Pomrenke.

The authors are with the School of Electrical Engineering and Computer Science, Oregon State University, Corvallis, OR 97331 USA (e-mail: gaoqi@oregonstate.edu; livermas@oregonstate.edu; wang@eecs.oregonstate.edu).

Color versions of one or more of the figures in this paper are available online at http://ieeexplore.ieee.org.

Digital Object Identifier 10.1109/JLT.2016.2631403

0733-8724 © 2016 IEEE. Personal use is permitted, but republication/redistribution requires IEEE permission.
See http://www.ieee.org/publications_standards/publications/rights/index.html for more information.

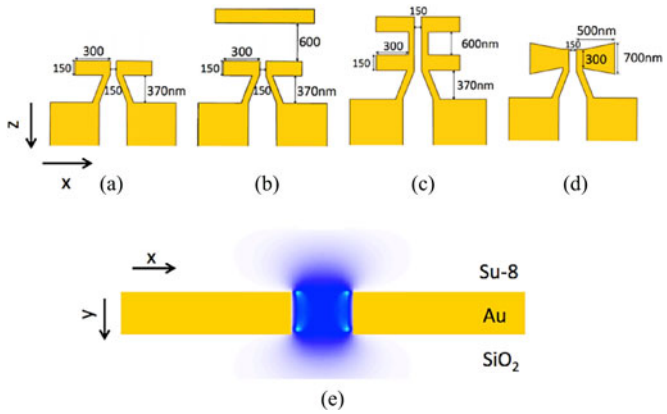

Fig. 1. Design of dipole antenna (a), Yagi-Uda antenna (b), dipole antenna array (c) and bowtie antenna (d); (e) Intensity of the optical field along x direction for a 1550 nm SPP mode.

the dipole-type antennas, the couple-in and couple-out efficiencies have been measured experimentally. Finally, the testing results of a plasmonic integrated circuit with these four types of antennas are presented by direct comparison of the couple-out efficiencies for these four antennas.

II. Design

A. Design of Nanoantenna Couplers

Due to the impedance mismatch and non-zero metal resistance of nanoantennas, free space incident radiation cannot be fully converted into the waveguide modes. However, by optimizing the design of nanoantenna, these losses can be minimized. In this paper, four types of nanoantennas have been studied. Our design of nanoantennas was simulated through the FullWave 3-D finite-difference time-domain (FDTD) method. The first nanoantenna is a dipole antenna shown in Fig. 1(a). The couple-in efficiency is maximized when it forms a standing wave along the antenna arms. This indicates that the length of the antenna arm should be an integer-number of the half wavelength. At optical frequencies, the standing wave along the metal surface is responding to a much shorter wavelength, which is called effective wavelength (λ_{eff}). The effective wavelength is determined by the plasmonic wavelength and geometry of the device. This is due to the fact that the radiation is not reflected from the metal surface, but penetrates into the metal and induces the oscillation of free electron gas. The λ_{eff} is calculated through the Eq. (1) from [39],

$$\lambda_{\text{eff}} = n_1 + n_2[\lambda/\lambda_p] \tag{1}$$

where λ_p is the plasma wavelength, n_1 and n_2 are coefficients related to the material properties and antenna geometry. In our case, for a free space wavelength of 1550 nm, the λ_{eff} is 1120 nm. λ_{eff} / 2 = 560 nm gives us a good starting point. After optimization through FDTD simulation and consideration of fabrication feasibility, we chose the total length of the antenna arm to be 600 nm to obtain a resonant wavelength and thus achieve an optimal coupling efficiency. The two $\lambda_{\text{eff}}/4$ antennas are separated by a small feed gap of 150 nm. Narrowing the feed gap can further increase the couple-in efficiency. The other requirement for maximum power transmission is to match the impedance between the half-wave dipole antenna and the plasmonic slot waveguide. In order to achieve impedance matching, a waveguide taper is used to smoothly connect the nanoantenna and the slot waveguide. The taper length is optimized based on the slot width of the waveguide, feed gap, and geometry of the nanoantenna. The final design parameters are shown in Fig. 1(a). For a Yagi-Uda antenna, a reflector is added to further improve the couple-in efficiency, which is placed 600 nm away in parallel to the dipole antenna. It can reflect the electromagnetic wave constructively back into the dipole antenna. The combination of the dipole antenna with a reflector is called Yagi-Uda antenna as shown in Fig. 1(b). Instead of using a reflector, we add one more dipole antenna in parallel to the original one to form a broadside antenna array, namely dipole antenna array, as shown in Fig. 1(c). The separation of these two array elements are chosen as $\lambda_{\text{eff}}/2$ to cancel out the radiation along the symmetric axis. There should be no phase difference between these two elements. The operating frequency of these three dipole-type antennas is determined by the physical length. In this case, the length should be equal to half wavelength, which can achieve good coupling efficiencies centered at the designed wavelength. The fourth type of nanoantenna is the bowtie antenna. It has a relatively broadband response. For the bowtie antenna, the design parameter is the angle of the fan-out shape plane. Here we implemented a bowtie antenna at 1550 nm operating wavelength, as illustrated in Fig. 1(d).

B. Design of Plasmonic Slot Waveguides

It has shown that plasmonic waveguides have high propagation loss. There is a tradeoff between the field confinement and the propagation length. In this paper we picked the slot width to be 300 nm and the Au film thickness to be 200 nm to minimize the propagation loss and maintain a high mode confinement as well. The electric field distribution, as shown in Fig. 1(e), illustrates that most of the optical field is confined within the gap.

III. Simulation Results

In our simulation, a 1.5 μm × 1.5 μm focused Gaussian beam is placed 100 nm above the Yagi-Uda antenna to approximate the excitation from a high numerical aperture (NA) optical fiber. In our analysis, as shown in Fig. 2(a), we define the total incident optical power as P_{in}, and the coupled optical power at the end of the input waveguide taper as P_1, and the transmitted power through the nanoantennas into the quartz substrate as T_{in}, and the waveguide mode power at the beginning of the output waveguide taper as P_2, and the optical power radiated out from the nanoantennas into air and the quartz substrate as P_{out} and T_{out}, respectively. The couple-in and couple-out efficiency are defined as:

$$CE_{\text{in}} = P_1/P_{\text{in}} \times 100\% \tag{1}$$

$$CE_{\text{out1}} = T_{\text{Out}}/P_2 \times 100\% \tag{2}$$

$$CE_{\text{out2}} = P_{\text{Out}}/P_2 \times 100\% \tag{3}$$

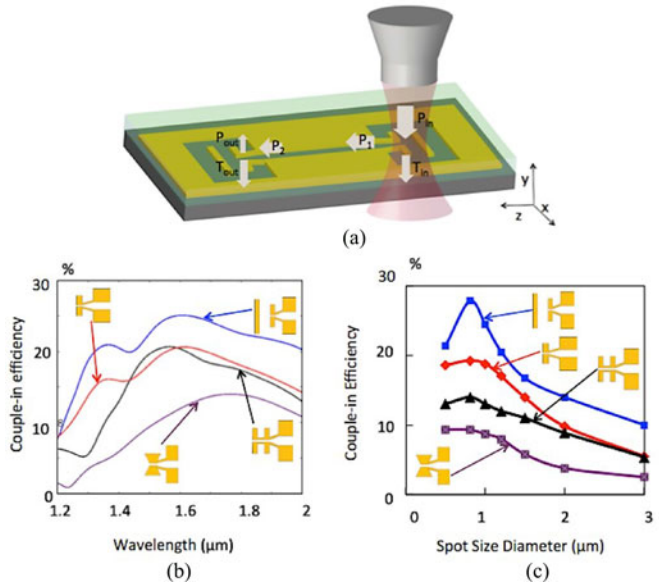

Fig. 2. (a) Schematic of optical coupling into plasmonic slot waveguide using dipole antennas from optical fibers; (b) Simulated optical coupling efficiency as a function of the incident optical wavelength; (c) Simulated couple-in efficiency as a function of the spot diameter.

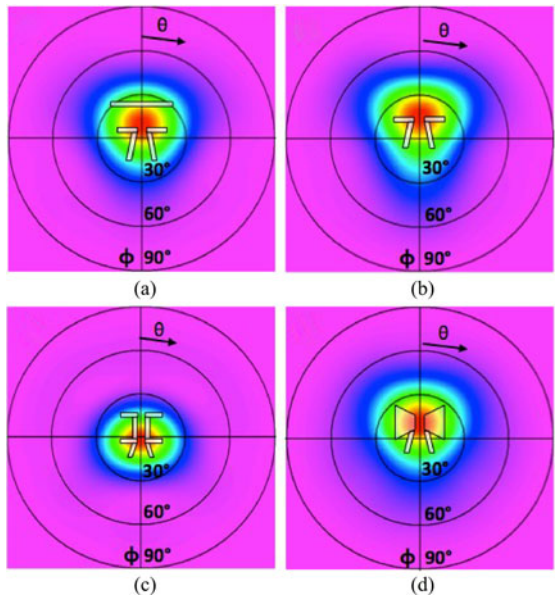

Fig. 3. Far field radiation patterns for Yagi-Uda antenna (a), dipole antenna (b), dipole antenna array (c), and bowtie antenna (d).

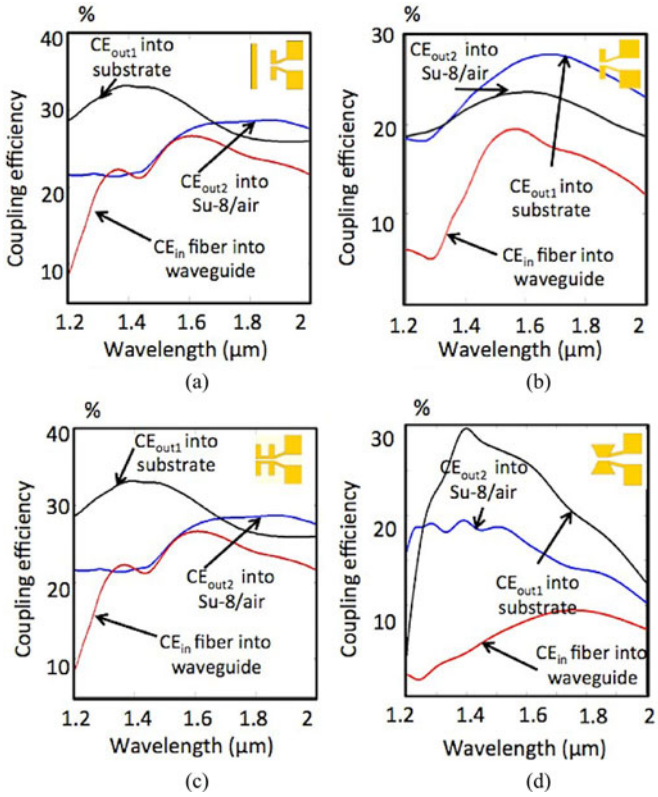

Fig. 4. Simulated couple-in and couple-out efficiency for Yagi-Uda antenna (a), dipole antenna (b), dipole antenna array (c), and bowtie antenna (d).

Fig. 2(b) shows the calculated couple-in efficiency. The maximum couple-in efficiency is 30%. We can see that adding a reflector can substantially increase the couple-in efficiency. The dipole antenna and the dipole antenna array have comparable couple-in efficiencies. The transmission spectrum of our bowtie antenna confirms its broad response ranging from 1.4 μm to 3 μm (2 μm to 3 μm range is not shown here.). We also explore the coupling efficiency as a function of incident radiation area. The results are shown in Fig. 2(c). The antenna can only capture the radiation within the effective area. Due to the limited effective area of antennas, the couple-in efficiency drops as the incident area increases. For the dipole-type antenna, the effective area is independent of the physical dipole length and only determined by the incident wavelength. However, the couple-in efficiency decreases when the incident radiation area is smaller than the effective area. This is due to the highly divergent angle of the incident beam exceeding the acceptance angle of the antenna. Fig. 3 shows the far-field radiation patterns. All of these antennas emit light with strong directionality within a polar cone of 30°. Among all of them, the dipole antenna array has the smallest radiation angle.

Based on the reciprocity theorem for the passive system, the radiation pattern of a receiving antenna is identical with that of transmission. We use the same design for both the receiving antenna and the transmitting antenna, and the couple-out efficiencies as a function of wavelength for all of the four antennas are also shown in Fig. 4(a)–(d). Based on reciprocity invariant theory, $\mathrm{CE_{in}}$ should be equal to $\mathrm{CE_{out2}}$ at all wavelengths. However, the couple-out efficiency is slightly higher than the couple-in efficiency. That is because at the receiving antenna there is a mode mismatch between the waveguide mode and the incident radiation mode, but no mode mismatch exists when the power is coupled out into the free space, so the couple-out efficiency is higher than the couple-in efficiency. For our designed Yagi-Uda antenna, the couple-in efficiency $\mathrm{CE_{in}}$ can achieve 25% and the couple-out efficiency into Su-8/air and the quartz substrate are 26% and 31%. The dipole antenna and dipole antenna array have similar couple-in efficiency, which is around 17%. The couple-out efficiency for dipole antenna is 45% and it is 35% for the dipole antenna array. Though

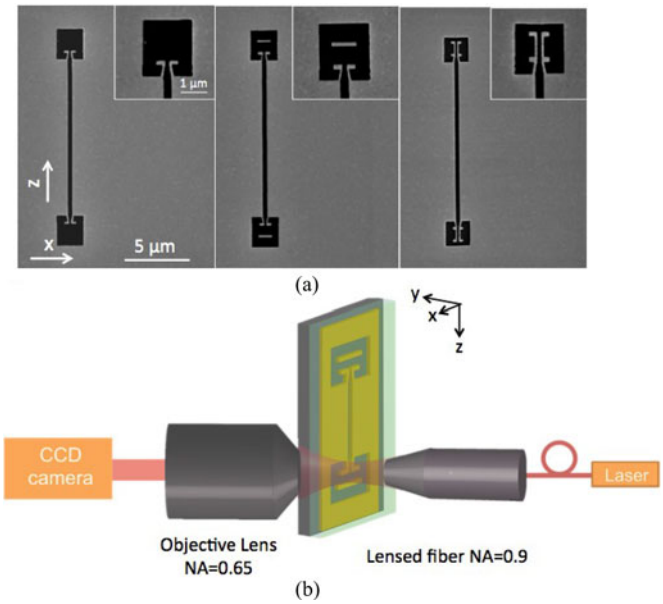

Fig. 5. (a) SEM image of the fabricated 10 μm plasmonic slot waveguide with the zoomed view of the dipole antenna, Yagi-Uda antenna, and dipole antenna array; (b) Configuration of the experimental setup.

coupling efficiency of the bowtie antenna is lower than others, it can cover wider wavelength range. On the basis of our simulation results, we found that the ratio of $\mathrm{T_{in}/P_1} = 4.4$ for our designed Yagi-Uda antenna. For the couple-out efficiency, the ratio of $\mathrm{T_{out}/P_{out}}$ will remain constant, since this ratio is only determined by the effective refractive indices of the top cladding and the substrate. When the top Su-8 cladding is 500 nm thick in our design, $\mathrm{T_{out}/P_{out}} = 1.2$. We also obtain the ratio of $\mathrm{T_{in}/P_1}$ and $\mathrm{T_{out}/P_{out}}$ for the dipole antenna and the dipole antenna array. Those numbers can be used to calculate the couple-in and couple-out efficiencies.

IV. Experimental Parts

A. Fabrication of Straight Waveguides with Dipole Type Nano-antenna Couplers

To thoroughly study the performance of different dipole- type antennas, we first fabricated straight plasmonic waveguides integrated with the dipole antenna, the Yagi-Uda antenna, and the dipole antenna array. We started the fabrication processes by cleaning a $1'' \times 1''$ 500 μm thick polished quartz substrate with acetone, isopropyl alcohol, and de-ionized water. A 220 nm gold thin film was deposited by thermal evaporation with a deposition rate at 5 Å/s. The device was then patterned by a 30 KV focused-ion beam (FIB) (Quanta 3D, FEI Company) lithography system with slot width of 300 $\pm$ 10 nm. To minimize the background signal, the receiving (couple-in) and transmitting (couple-out) antennas were patterned within a 1.5 μm $\times$ 1.5 μm window as shown in Fig. 5(a). The window has only slight effects on the radiation pattern and coupling efficiency, which is verified by the simulation results. Following the FIB process, Su-8 was spin-coated and then hard baked for 20 min at 200 °C to form a 500 nm thick top cladding. Straight waveguides integrated with the dipole antenna, the Yagi-Uda antenna and the dipole antenna array with different lengths (L = 10 μm, 15 μm, 20 μm and 30 μm) were fabricated using the same fabrication settings. The scanning electron microscopy (SEM) image in Fig. 5(a) depicts the fabricated 10 μm plasmonic slot waveguide with the zoomed view of the Yagi-Uda antenna, dipole antenna, and dipole antenna array.

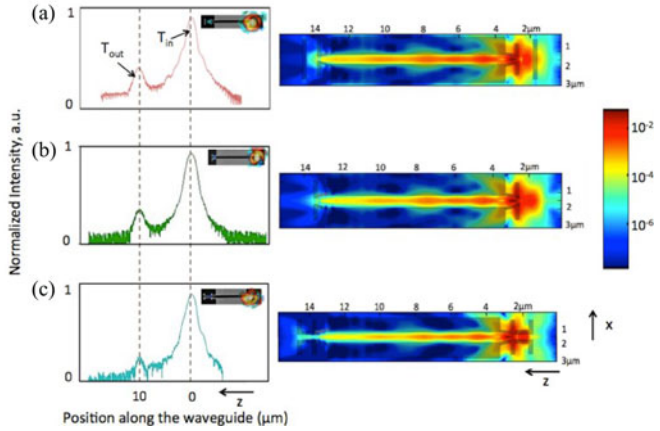

Fig. 6. Simulated near-field distribution and measured optical intensity profile in log scale of plasmonic slot waveguide with Yagi-Uda antenna (a), dipole antenna (b), dipole antenna array (c), and the inset figures show the SEM images of each device and the near field images of the 10 μm waveguides.

The optical characterization system is shown in Fig. 5(b). The sample was mounted on a three-dimensional translation/rotation stage, allowing highly precise angular adjustment and spatial alignment in regards to the incident light spot. Light from a 1.55 μm laser was coupled into a single-mode polarization-maintaining (PM) fiber with high numerical aperture of 0.9 (PROFA 1-D from Chiral Photonics, Inc.). It utilizes a "vanishing core" concept to achieve such high NA [39]. The high NA fiber is capable of focusing the beam spot to a minimum size of 2 μm $\times$ 2 μm and can be precisely aligned to the receiving nanoantenna through monitoring the output power from the transmitting antenna. The incident radiation is polarized along the antenna arms, designated as the transverse electric (TM) to the plasmonic slot waveguide. All the transmitted light $(\mathrm{T_{out}} + \mathrm{T_{in}})$ is collected by an objective lens with NA = 0.65 on the other side of sample, and was then monitored by a CCD camera.

B. Characterization of Straight Waveguides with Dipole Type Nanoantenna Couplers

Fig. 6(a)–(c) presents the measured intensity profile along the 10 μm plasmonic slot waveguide, compared with the simulated near-field distribution. The higher peak represents the direct transmitted incident light $(\mathrm{T_{in}})$ and the lower one denotes the light radiated into the substrate $(\mathrm{T_{out}})$, and the light between these two peaks comes from the optical scattering of the slot waveguide. The insert figures illustrate the near field image of the straight waveguides. The optical power of $\mathrm{T_{in}}$ and $\mathrm{T_{out}}$ can be obtained by integration of the intensity data from the camera along the waveguide. The total incident power $\mathrm{P_{in}}$ from the high NA fiber can be measured by the transmitted light through the open window without an antenna (1.5 μm $\times$ 1.5 μm), which is –

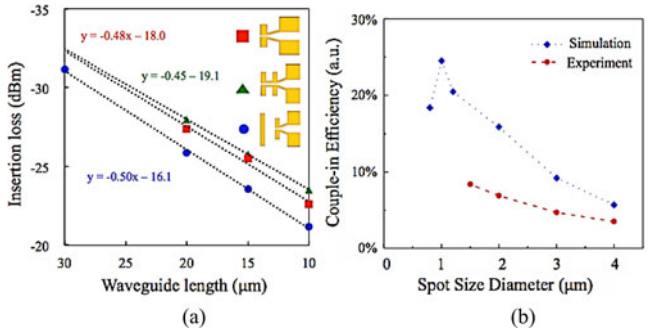

Fig. 7. (a) Measured output power for plasmonic slot waveguides with different lengths; (b) Simulated and measured couple-in efficiency for Yagi-Uda antenna as a function of the spot diameter.

TABLE I
SIMULATION AND EXPERIMENTAL RESULTS FOR YAGI-UDA ANTENNA, DIPOLE ANTENNA AND DIPOLE ANTENNA ARRAY

	Couple-in efficiency		Total couple-out efficiency	
	Simulation results	Experimental results	Simulation results	Experimental results
Yagi-Uda antenna	25%	8.6%	57%	46%
Dipole antenna	17%	6%	45%	40%
Dipole antenna array	17%	6%	35%	30%

7.7 dBm. For the 10 μm waveguide with the Yagi-Uda antenna, the measured $\mathrm{T_{in}}$ is –11.96 dBm and $\mathrm{T_{out}}$ is –21.19 dBm. After measuring the $\mathrm{T_{out}}$ from all of these waveguides with different lengths, we plotted the data in Fig. 7(a) with a linear fitting curve. The average propagation loss, which is the slope of the linear fitting curve, is determined to be 0.47 dB/μm, which is higher than the simulation result of 0.3 dB/μm. This is possibly due to FIB lithography induced roughness on sidewalls of the slot and higher ohmic losses of thin gold film than the ideal permittivity. For the Yagi-Uda antenna, the couple-in and couple-out efficiencies can be calculated by utilizing the ratio of $\mathrm{T_{in}/P_1} = 4.4$ and $\mathrm{T_{out}/P_{out}} = 1$ from simulation, which are 8.6% and 46% total couple-out efficiency (23% to air and 23% to the substrate) on average. In order to further increase the optical coupling efficiency, we may follow the approach as pointed out in [36] to reduce the gap width of the plasmonic nanoantennas in our future work. The couple-in and couple-out efficiencies of the other two nanoantennas can be calculated in the same approach. The dipole antenna and dipole antenna array have similar couple-in efficiency, which is around 6%. The couple-out efficiency for dipole antenna is 40% and it is 30% for dipole antenna array. The simulation and experimental results of different types of nanoantennas are summarized in Table I.

We also characterized the dependence of the couple-in efficiency of the Yagi-Uda nanoantenna with the incident beam spot by varying the size of the incident beam spot. Since the light from the high NA fiber is highly divergent, the incident beam spot size can be enlarged by moving the fiber away and then measured by the optical beam profiler. The minimum beam spot size from the high NA fiber is 2 μm. However, with the confinement of the optical window, we can normalize the incident beam spot to 1.5 μm. We measured $\mathrm{T_{out}}$ with different incident spot diameters of 1.5 μm, 2 μm, 3 μm and 4 μm, and the experimentally measured data of the couple-in efficiency is plotted in Fig. 7(b). The overall trend matches the simulation results very well. However, the lower experimental couple-in efficiencies compared to the simulation results possibly comes from 1) the optical loss of the thermally evaporated gold film is much larger than the perfect gold film being used in the simulation [40]; 2) the surface-roughness and other fabrication imperfection of the plasmonic nanoantennas; 3) the slight misalignment in the optical characterization.

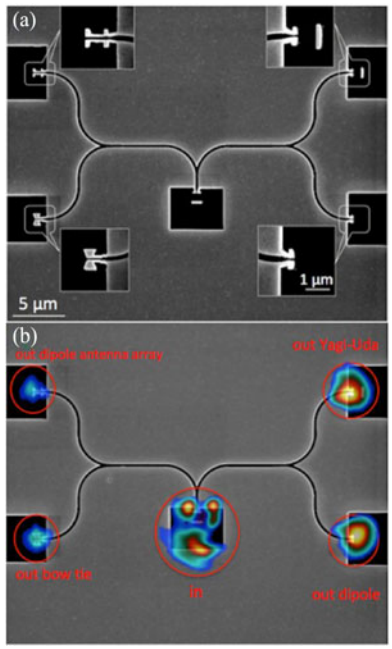

Fig. 8. (a) SEM image of the photonic integrated circuit; (b) Near-field image of the plasmonic circuit.

C. Design, Fabrication, and Characterization of Plasmonic Integrated Circuit

The designed plasmonic integrated circuit consists of an input plasmonic waveguide with a Yagi-Uda antenna, and the input waveguide is split by two-stage cascaded Y-splitters into four output waveguides: one with the Yagi-Uda antenna, one with the dipole antenna, one with the dipole antenna array, and one bowtie antenna. The propagating light can be split equally by the Y-splitter. Thus, besides the scattering loss and propagation loss, the incident power is equally divided into four branches and the same amount of power is delivered to these four transmitting antennas, so we can directly compare the couple-out efficiencies of all four antennas by measuring the amount of the radiating power. The bending radius was optimized to achieve a negligible bending loss. In order to reduce the total propagation length, thus reducing the propagation loss, we set the bending radius of the plasmonic integrated circuit to be 3 μm and the bending loss is 1.4 dB from the simulation result.

The plasmonic integrated circuit was fabricated using the same fabrication settings as we used for the straight waveguides, except that we did not spin-coated Su-8. The SEM image

is shown in Fig. 8(a). The same setup is used to characterize the plasmonic integrated circuit. The light is coupled into the circuit through the input antenna and coupled out by four different antennas. The optical power of directly transmitted at the input nanoantenna and radiated power by four output nanoantennas into substrate can be obtained by integration of the intensity data from the CCD camera as shown in Fig. 8(b). By integration of the entire radiated area and subtraction of the background signals, we can obtain the radiated power ratio of different nanoantennas. $\mathrm{P_{out\,Yagi\text{-}Uda}}$: $\mathrm{P_{out\,dipole}}$: $\mathrm{P_{out\,dipole\,array}}$: $\mathrm{P_{out\,bowtie}} = 1.1 : 1.0 : 0.3 : 0.4$. The Yagi-Uda nanoantenna has the highest couple out efficiency, which is consistent with the simulation results.

V. Conclusion

In conclusion, we presented the design and performance of four types of antennas at 1.55 μm wavelength, which are dipole antenna, Yagi-Uda antenna, dipole antenna array, and bowtie antenna. The spectrum, coupling efficiency, far field radiation pattern are presented. We also quantitatively characterize the dependence of the couple-in efficiency to the spot size of the incident light. For dipole-type antennas, we experimentally measured the couple-in and couple-out efficiencies. Moreover, we designed and fabricated plasmonic integrated circuit corporation with the designed four types of antennas. And the direct and efficient optical coupling from an optical fiber into plasmonic integrated circuits is demonstrated as well. Direct comparison of the couple-out efficiencies of four antennas is illustrated.

References

[1] E. Ozbay, "Plasmonics: Merging photonics and electronics at nanoscale dimensions," *Science*, vol. 311, no. 5758, pp. 189–193, 2006.

[2] V. J. Sorger, R. F. Oulton, R.-M. Ma, and X. Zhang, "Toward integrated plasmonic circuits," *MRS Bull.*, vol. 37, no. 8, pp. 728–738, 2012.

[3] J. A. Schuller, E. S. Barnard, W. Cai, Y. C. Jun, J. S. White, and M. L. Brongersma, "Plasmonics for extreme light concentration and manipulation," *Nature Mater.*, vol. 9, no. 3, pp. 193–204, 2010.

[4] R. Zia, J. A. Schuller, A. Chandran, and M. L. Brongersma, "Plasmonics: The next chip-scale technology," *Mater. Today*, vol. 9, no. 7, pp. 20–27, 2006.

[5] D. K. Gramotnev and S. I. Bozhevolnyi, "Plasmonics beyond the diffraction limit," *Nature Photon.*, vol. 4, no. 2, pp. 83–91, 2010.

[6] K. C. Huang, M.-K. Seo, T. Sarmiento, Y. Huo, J. S. Harris, and M. L. Brongersma, "Electrically driven subwavelength optical nanocircuits," *Nature Photon.*, vol. 8, no. 3, pp. 244–249, 2014.

[7] R. Service, "Nanolasers. Ever-smaller lasers pave the way for data highways made of light," *Science*, vol. 328, no. 5980, pp. 810–811, 2010.

[8] R. F. Oulton *et al.*, "Plasmon lasers at deep subwavelength scale," *Nature*, vol. 461, no. 7264, pp. 629–632, 2009.

[9] M. Noginov *et al.*, "Demonstration of a spaser-based nanolaser," *Nature*, vol. 460, no. 7259, pp. 1110–1112, 2009.

[10] S.-H. Kwon *et al.*, "Subwavelength plasmonic lasing from a semiconductor nanodisk with silver nanopan cavity," *Nano Lett.*, vol. 10, no. 9, pp. 3679–3683, 2010.

[11] H. A. Atwater and A. Polman, "Plasmonics for improved photovoltaic devices," *Nature Mater.*, vol. 9, no. 3, pp. 205–213, 2010.

[12] E. Hutter and J. H. Fendler, "Exploitation of localized surface plasmon resonance," *Adv. Mater.*, vol. 16, no. 19, pp. 1685–1706, 2004.

[13] K. M. Mayer and J. H. Hafner, "Localized surface plasmon resonance sensors," *Chem. Rev.*, vol. 111, no. 6, pp. 3828–3857, 2011.

[14] Y. Liu, J.-J. Yin, and Z. Nie, "Harnessing the collective properties of nanoparticle ensembles for cancer theranostics," *Nano Res.*, vol. 7, no. 12, pp. 1719–1730, 2014.

[15] L. Li, U. Steiner, and S. Mahajan, "Single nanoparticle SERS probes of ion intercalation in metal-oxide electrodes," *Nano Lett.*, vol. 14, no. 2, pp. 495–498, 2014.

[16] Y. B. Zheng, B. Kiraly, S. Cheunkar, T. J. Huang, and P. S. Weiss, "Incident-angle-modulated molecular plasmonic switches: A case of weak exciton–plasmon coupling," *Nano Lett.*, vol. 11, no. 5, pp. 2061–2065, 2011.

[17] Y. B. Zheng *et al.*, "Active molecular plasmonics: controlling plasmon resonances with molecular switches," *Nano Lett.*, vol. 9, no. 2, pp. 819–825, 2009.

[18] D. Pacifici, H. J. Lezec, and H. A. Atwater, "All-optical modulation by plasmonic excitation of CDSE quantum dots," *Nature Photon.*, vol. 1, no. 7, pp. 402–406, 2007.

[19] M. Liu *et al.*, "A graphene-based broadband optical modulator," *Nature*, vol. 474, no. 7349, pp. 64–67, 2011.

[20] S. K. Pickus, S. Khan, C. Ye, Z. Li, and V. J. Sorger, "Silicon plasmon modulators: Breaking photonic limits," *IEEE Photon. Soc., Res. Highlights*, vol. 27, no. 6, pp. 4–10, Dec. 2013.

[21] W. Cai, J. S. White, and M. L. Brongersma, "Compact, high-speed and power-efficient electrooptic plasmonic modulators," *Nano Lett.*, vol. 9, no. 12, pp. 4403–4411, 2009.

[22] H. W. Lee *et al.*, "Nanoscale conducting oxide plasmostor," *Nano Lett.*, vol. 14, no. 11, pp. 6463–6468, 2014.

[23] J. N. Anker, W. P. Hall, O. Lyandres, N. C. Shah, J. Zhao, and R. P. Van Duyne, "Biosensing with plasmonic nanosensors," *Nature Mater.*, vol. 7, no. 6, pp. 442–453, 2008.

[24] N. P. DeLeon, M. D. Lukin, and H. Park, "Quantum plasmonic circuits," *IEEE J. Sel. Topics Quantum Electron.*, vol. 18, no. 6, pp. 1781–1791, Nov./Dec. 2012.

[25] T. Aihara *et al.*, "Coherent plasmonic interconnection in silicon-based electrical circuit," *J. Lightw. Technol.*, vol. 33, no. 10, pp. 2139–2145, May 2015.

[26] C. Ropers, C. Neacsu, T. Elsaesser, M. Albrecht, M. Raschke, and C. Lienau, "Grating-coupling of surface plasmons onto metallic tips: A nanoconfined light source," *Nano Lett.*, vol. 7, no. 9, pp. 2784–2788, 2007.

[27] M. G. Nielsen and S. I. Bozhevolnyi, "Highly confined gap surface plasmon modes in metal strip–gap–film configurations," *JOSA B*, vol. 32, no. 3, pp. 462–467, 2015.

[28] B. Arigong *et al.*, "Design of wide-angle broadband luneburg lens based optical couplers for plasmonic slot nano-waveguides," *J. Appl. Phy.*, vol. 114, no. 14, 2013, Art. no. 144301.

[29] S. Zhang, C. Gu, and H. Xu, "Single nanoparticle couplers for plasmonic waveguides," *Small*, vol. 10, no. 21, pp. 4264–4269, 2014.

[30] A. Andryieuski, V. A. Zenin, R. Malureanu, V. S. Volkov, S. I. Bozhevolnyi, and A. V. Lavrinenko, "Direct characterization of plasmonic slot waveguides and nanocouplers," *Nano Lett.*, vol. 14, no. 7, pp. 3925–3929, 2014.

[31] F. Obelleiro, J. Taboada, D. Solís, and L. Bote, "Directive antenna nanocoupler to plasmonic gap waveguides," *Opt. Lett.*, vol. 38, no. 10, pp. 1630–1632, 2013.

[32] J.-S. Huang, T. Feichtner, P. Biagioni, and B. Hecht, "Impedance matching and emission properties of nanoantennas in an optical nanocircuit," *Nano Lett.*, vol. 9, no. 5, pp. 1897–1902, 2009.

[33] L. Novotny and N. van Hulst, "Antennas for light," *Nature Photon.*, vol. 5, no. 2, pp. 83–90, 2011.

[34] A. Andryieuski, R. Malureanu, G. Biagi, T. Holmgaard, and A. Lavrinenko, "Compact dipole nanoantenna coupler to plasmonic slot waveguide," *Opt. Lett.*, vol. 37, no. 6, pp. 1124–1126, 2012.

[35] A. Kriesch, S. P. Burgos, D. Ploss, H. Pfeifer, H. A. Atwater, and U. Peschel, "Functional plasmonic nanocircuits with low insertion and propagation losses," *Nano Lett.*, vol. 13, no. 9, pp. 4539–4545, 2013.

[36] A. Andryieuski, R. Malureanu, J.-S. Bouillard, A. V. Zayats, and A. V. Lavrinenko, "Improving plasmonic waveguides coupling efficiency using nanoantennas," in *Proc. 14th Int. Conf. Transparent Opt. Netw.*, 2012, pp. 1–4.

[37] C. A. Balanis, *Antenna Theory: Analysis and Design*. New York, NY, USA: Wiley, 1997.

[38] L. Novotny, "Effective wavelength scaling for optical antennas," *Phys. Rev. Lett.*, vol. 98, no. 26, Jun. 2007, Art. no. 266802.

[39] V. I. Kopp, J. Park, M. Wlodawski, J. Singer, D. Neugroschl, and A. Z. Genack, "Chiral fibers: Microformed optical waveguides for polarization control, sensing, coupling, amplification, and switching," *J. Lightw. Technol.*, vol. 32, no. 4, pp. 605–613, Feb. 2014.

[40] F. Ren, X. Wang, and A. X. Wang, "Thermo-optic modulation of plasmonic bandgap on metallic photonic crystal slab," *Appl. Phy. Lett.*, vol. 102, no. 18, May 2013, Art. no. 181101.

Qian Gao received the B.E. degree in material science and engineering from the University of Science and Technology, Beijing, China, in 2012 and the M.S. degree in material science and engineering from the University of Pennsylvania, Philadelphia, PA, USA, in 2014. She is currently working toward the Ph.D. degree in electrical engineering, Oregon State University, Corvallis, OR, USA. Her current research interests include plasmonic nanophotonic devices and electric-optical modulators.

Spencer Liverman received the B.S. degree in electrical engineering from the School of Electrical Engineering and Computer Science, Oregon State University, Corvallis, OR, USA, in 2014, where he is currently working toward the Ph.D. degree in electrical engineering. His research interests include hybrid indoor free-space communication networks that combine both optical and WiFi technologies. He is the President of Student Chapter of Optical Society of America in Oregon State University.

Alan X. Wang received the Ph.D. degree in electrical and computer engineering from the University of Texas, Austin, TX, USA, in 2006. Since 2011, he has been an Assistant Professor in the School of Electrical Engineering and Computer Science, Oregon State University, Corvallis, OR, USA. From 2007 to 2011, he was with Omega Optics, Inc., where he served as the Chief Research Scientist for 9 SBIR/STTR projects. His research interests include nanophotonic devices for optical interconnects and optical sensors for chemical and biological detection. His current research activities are sponsored by the National Science Foundation, the National Institutes of Health, Oregon Nanoscience and Microtechnologies Institute, the National Energy Technology Laboratory, and industrial sponsors such as Hewlett-Packard. He has more than 70 journal publications and 70 conference presentations, and also holds three U.S. patents. He is a Senior Member of the IEEE Photonics, SPIE, and Optical Society of America.